LARGE EDDY SIMULATION OF SUPERSONIC TURBULENT FLOW IN EXPANSION-COMPRESSION CORNER

DOYLE KNIGHT and HONG YAN
Rutgers - The State University of New Jersey
Piscataway, NJ 08854

ALEXANDER ZHELTOVODOV
Institute of Theoretical and Applied Mechanics
630090 Novosibirsk, Russia

Abstract A Large Eddy Simulation (LES) methodology has been developed for supersonic turbulent flows with strong shock boundary layer interaction. Results are presented for an expansion-compression corner at Mach 3 and compared with experimental data.

Introduction

The interaction of shock waves and turbulent boundary layers is a common and important phenomenon in aerodynamics, and has been studied extensively (Settles and Dolling, 1990; Zheltovodov, 1996). Conventional Reynolds-averaged Navier-Stokes methods have been unable to accurately predict separated shock wave turbulent boundary layer interactions (Knight and Degrez, 1998). Recently, Large Eddy Simulation (LES) and Direct Numerical Simulation (DNS) have been applied to shock wave turbulent boundary layer interactions with significant success. Examples include Adams, 1998, Urbin et al., 1999, Rizzetta et al., 2000 and Rizzetta and Visbal, 2001.

The objective of this paper is to assess the capability of our LES methodology to accurately predict the flowfield in a supersonic expansion-compression corner (Fig. 1). This configuration is reminiscent of aerodynamic configurations wherein a supersonic boundary layer is subjected to an initial expansion followed by a subsequent compression. Interest in this configuration is due in part to the stabilizing influence of the expansion (Dussauge and Gaviglio, 1987; Zheltovodov et al., 1987; Zhel-

tovodov and Schuelein, 1988; Smith and Smits, 1997; Stephen et al., 1998; Zheltovodov et al., 1990b). The first systematic combined experimental and numerical study of an expansion-compression corner by Zheltovodov et al., 1992 and Zheltovodov et al., 1993 showed that several different turbulence models (including $k-\epsilon$, $q-\omega$ and several modifications thereto) did not accurately predict the separation and attachment positions, and distributions of surface skin friction and heat transfer. We therefore seek to ascertain the capability of LES to predict this flowfield.

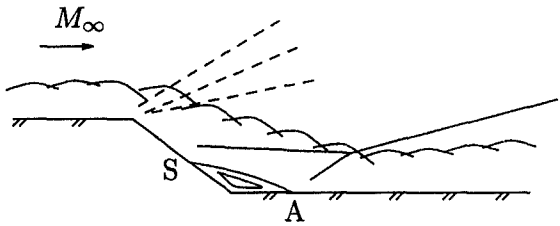

Figure 1. Expansion-compression corner

Governing Equations

The governing equations are the spatially filtered, Favre-averaged compressible Navier-Stokes equations. The spatial filtering removes the small scale (*subgrid scale*) fluctuations, while the three dimensional, time dependent large scale (*resolved scale*) motion is retained. For an arbitrary function $\mathcal{F}(x_i,t)$, the ordinary and Favre-filtered variables $\overline{\mathcal{F}}(x_i,t)$ and $\widetilde{\mathcal{F}}(x_i,t)$ are

$$\overline{\mathcal{F}}(x_i,t) = \int_D G(x_i-\xi_i,\Delta)\,\mathcal{F}(\xi_i,t)\,d\xi_i \quad \text{and} \quad \widetilde{\mathcal{F}}(x_i,t) = \frac{\overline{\rho\mathcal{F}}}{\bar{\rho}} \tag{1}$$

where G is the filter function, and Δ is a measure of the filter width and is related to the computational mesh size.

The filtered governing equations using Cartesian tensor notation are

$$\frac{\partial\bar{\rho}}{\partial t} + \frac{\partial\bar{\rho}\tilde{u}_i}{\partial x_i} = 0 \tag{2}$$

$$\frac{\partial\bar{\rho}\tilde{u}_i}{\partial t} + \frac{\partial\bar{\rho}\tilde{u}_i\tilde{u}_j}{\partial x_j} = -\frac{\partial\bar{p}}{\partial x_i} + \frac{\partial\mathcal{T}_{ij}}{\partial x_j} \tag{3}$$

$$\frac{\partial\bar{\rho}\tilde{e}}{\partial t} + \frac{\partial}{\partial x_j}\left(\bar{\rho}\tilde{e}+\bar{p}\right)\tilde{u}_j = \frac{\partial\mathcal{H}_j}{\partial x_j} \tag{4}$$

$$\bar{p} = \bar{\rho}R\tilde{T} \tag{5}$$

where x_i represents the Cartesian coordinates ($i = 1, 2, 3$), $\bar{\rho}$ is the mean density, $\tilde{u}_i$ are the Cartesian components of the filtered velocity and $\bar{p}$ is the mean pressure. The total stress tensor $\mathcal{T}_{ij} = \tau_{ij} + \bar{\sigma}_{ij}$ where the Subgrid Scale (SGS) stress τ_{ij} and viscous stress $\bar{\sigma}_{ij}$ are

$$\begin{aligned} \tau_{ij} &= -\bar{\rho}\left(\widetilde{u_i u_j} - \tilde{u}_i \tilde{u}_j\right) \\ \bar{\sigma}_{ij} &= \mu(\tilde{T})\left(-\frac{2}{3}\frac{\partial \tilde{u}_k}{\partial x_k}\delta_{ij} + \frac{\partial \tilde{u}_i}{\partial x_j} + \frac{\partial \tilde{u}_j}{\partial x_i}\right) \end{aligned} \tag{6}$$

where $\mu(\tilde{T})$ is the molecular viscosity. The sum of the heat flux plus work done by the stresses is $\mathcal{H}_j = Q_j + \bar{q}_j + \mathcal{T}_{ij}\tilde{u}_i$ where the SGS and molecular heat fluxes are

$$Q_j = -c_p \bar{\rho}\left(\widetilde{u_j T} - \tilde{u}_j \tilde{T}\right) \quad \text{and} \quad \bar{q}_j = \kappa(\tilde{T})\frac{\partial \tilde{T}}{\partial x_j} \tag{7}$$

where $\kappa(\tilde{T})$ the molecular thermal conductivity. The form of $\mathcal{H}_j$ was proposed by Knight et al., 1998 and found to provide an accurate model of SGS turbulent diffusion in decaying compressible isotropic turbulence (Martin et al., 1999). The total energy $\bar{\rho}\tilde{e}$ and SGS turbulence kinetic energy $\bar{\rho}k$ per unit volume are

$$\bar{\rho}\tilde{e} = \bar{\rho}c_v\tilde{T} + \tfrac{1}{2}\bar{\rho}\tilde{u}_i\tilde{u}_i + \bar{\rho}k \quad \text{and} \quad \bar{\rho}k = \tfrac{1}{2}\bar{\rho}\left(\widetilde{u_i u_i} - \tilde{u}_i\tilde{u}_i\right) \tag{8}$$

Closure of the system of equations (2) to (5) requires specification of a model for the subgrid scale stress τ_{ij} and heat flux Q_j. There are two basic approaches (Ghosal, 1999), namely, 1) the explicit specification of an SGS model, and 2) the Monotone Integrated Large Eddy Simulation (MILES) method. In first approach, an explicit mathematical model for τ_{ij} and heat flux Q_j is defined (*e.g.*, the Smagorinsky model). Examples are presented in the recent reviews of Galperin and Orszag, 1993 and Lesieur and Métais, 1996. In the second approach, the SGS model is inherent in the numerical algorithm (Boris et al., 1992; Oran and Boris, 1993; Grinstein, 1996; Grinstein and Fureby, 1998; Fureby and Grinstein, 2000). Fureby and Grinstein, 1999 showed that MILES introduces a tensor eddy diffusivity into the equivalent SGS stress, in contrast to the isotropic eddy diffusivity of the standard explicit Smagorinsky-type SGS models.

The no-slip condition is applied at solid (impermeable) boundaries. The downstream boundary condition for supersonic flows is typically a zero gradient condition on the conservative flow variables ($\bar{\rho}$, $\bar{\rho}\tilde{u}_i$, $\bar{\rho}\tilde{e}$). Periodic boundary conditions are usually employed for the spanwise boundaries with the requirement that the spanwise domain is large compared to the energy containing eddies of the flow and the flowfield is statistically homogeneous in the spanwise direction. The farfield boundary

condition for supersonic flows is typically a Riemann condition allowing waves to leave the computational domain without reflection. The inflow boundary condition for boundary layers is a time-dependent boundary layer profile obtained by the rescaling method originally developed by Lund et al., 1998 for incompressible boundary layers and extended to compressible boundary layers by Urbin and Knight, 1999. The initial condition is typically obtained by linear interpolation from a previous simulation at comparable Mach and Reynolds numbers.

Numerical Algorithm

The governing equations (2) to (5) are solved using a unstructured grid of tetrahedra. The finite volume algorithm is second order accurate in space and time. The inviscid fluxes are computed using Godunov's method with the left and right states at each face reconstructed using a second order Least Squares method (Okong'o and Knight, 1998a). The stencil of cells employed for reconstruction is isotropic except in the vicinity of shock waves where an ENO-like anisotropic stencil is employed (Chernyavsky et al., 2001). The MILES methodology is employed (*i.e.*, $\tau_{ij} = 0$, $Q_j = 0$). The molecular viscous stresses and heat flux are obtained using a discrete version of Gauss' Theorem (Okong'o and Knight, 1998a). The temporal integration is performed by using a second-order accurate Runge-Kutta method. The code is parallelized using domain decomposition with the Message Passing Interface (MPI). The flow variables are non-dimensionalized using the incoming boundary layer thickness δ, and incoming freestream velocity U_∞, density ρ_∞, static temperature T_∞ and molecular viscosity μ_∞.

The code has been validated for a variety of turbulent flows by comparison with experiment and Direct Numerical Simulation (DNS). Examples include decay of isotropic turbulence (Knight et al., 1997; Knight et al., 1998), incompressible channel flow (Okong'o and Knight, 1998b; Okong'o et al., 2000), supersonic turbulent boundary layer (Urbin et al., 1999; Urbin and Knight, 1999; Yan et al., 2000; Urbin and Knight, 2001), and supersonic compression corner (Urbin et al., 1999; Urbin et al., 2000; Yan et al., 2000; Chernyavsky et al., 2001). The supersonic boundary layer results are summarized in the next section.

Flat Plate Boundary Layer

Urbin and Knight, 2001 performed an LES of an adiabatic Mach 3 boundary layer. A detailed grid refinement study was performed to ascertain the required grid resolution in the viscous sublayer, logarithmic and outer regions of the boundary layer. The computed mean veloc-

ity profile, expressed in Van Driest transformed notation, is shown in Fig. 2. The profile shows excellent agreement with the logarithmic region of the Law of the Wall. The computed adiabatic wall temperature is within 3% of the empirical formula $T_{aw} = T_\infty \left(1 + \frac{1}{2}(\gamma - 1) Pr_{t_m} M_\infty^2\right)$ where $Pr_{t_m} = 0.89$ is the mean turbulent Prandtl number. The computed friction velocity u_τ is within 5% of the correlation obtained from the combined Law of the Wall and Wake. The computed normalized Reynolds shear stress $< \rho >< u''v'' > /\tau_w$, shown in Fig. 3, shows excellent agreement with the experimental data.

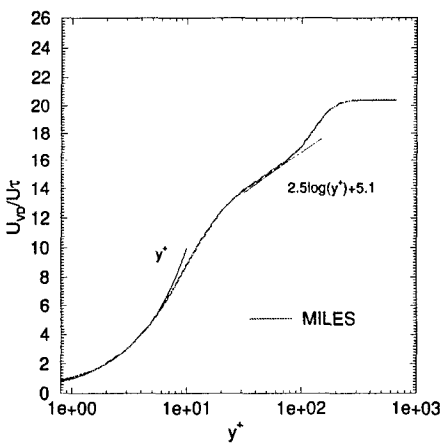

Figure 2. Mean Van Driest velocity

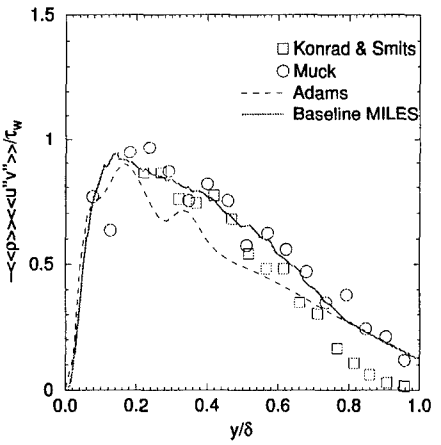

Figure 3. Reynolds shear stress

Expansion-Compression Corner

Details of Computation

The flowfield configuration is shown in Fig. 1. An incoming Mach 3 adiabatic equilibrium turbulent boundary layer of height δ expands over a 25° corner followed by a 25° compression. The distance along the expansion surface is 7.1δ (*i.e.*, the vertical distance between the two horizontal surfaces is 3δ, and the horizontal distance between the expansion and compression corners is 6.43δ).

The Cartesian coordinates x, y and z are aligned in the incoming streamwise, transverse and spanwise directions with the origin at the inflow boundary. The computational domain is $L_x = 24.0\delta$, $L_y = 3.4\delta$, and $L_z = 1.925\delta$. The expansion corner is located at 4δ from the inflow boundary. The grid consists of $253 \times 35 \times 57$ nodes in the x, y and

z directions, respectively, forming 479,808 hexahedra which are subdivided into five tetrahedra each. Thus, the total number of tetrahedra is 2,399,040. The grid is stretched in the y direction with spacing 0.008δ at the wall and a geometric stretching factor of 1.154. The grid is concentrated in the streamwise direction in the neighborhood of the expansion and compression corners. The details are shown in Table 1 where $\Delta y^+ = \Delta y u_\tau / \nu_w$ where ν_w is the computed kinematic viscosity at the wall, $u_\tau = \sqrt{\tau_w / \rho_w}$ is the friction velocity, τ_w is the computed wall shear stress and ρ_w is the computed density at the wall. The grid is consistent with the resolution requirements for the LES code established by Urbin and Knight, 2001.

Table 1. Details of Grid

Name	Δx^+	Δy^+ at the wall	Δz^+	$\Delta x/\delta$	$\Delta y/\delta$ at $y = \delta$	$\Delta z/\delta$	Tetras
Computed	20.9	1.67	7.1	0.1	0.14	0.034	2,399,040

The inflow boundary condition is obtained from a separate flat plate boundary layer computation. All the quantities are averaged in time and in the spanwise direction and denoted by $< f >$. The time averaging period is set to three times the flow-through time, where one flow-through time is defined as the time for the freestream flow to traverse the computational domain. The averaging is performed once the initial transient has decayed (*i.e.*, after four flow-through times). The details are presented in Urbin et al., 1999.

Experiments

Experimental data has been obtained by Zheltovodov et al., 1987, Zheltovodov and Schuelein, 1988, and Zheltovodov et al., 1990a and presented in part in tabular form in Zheltovodov et al., 1990b for the expansion-compression corner at Mach 3 and several Reynolds numbers Re_δ based on the incoming boundary layer thickness δ. The experimental conditions are listed in Table 2, where FPBL and ECC imply flat plate boundary layer and expansion-compression corner, respectively. The LES was performed at a lower Reynolds number ($Re_\delta = 2 \times 10^4$) than the experiment ($Re_\delta = 4.4 \times 10^4$ to 1.94×10^5) for reasons of computational cost. Additional LES cases will be performed at higher Reynolds numbers.

Table 2. Details of Experiments and Computation

Cases	Mach	Re_δ	References
ECC	2.9	4.07×10^4	Zheltovodov et al., 1990a
ECC	2.9	6.76×10^4	Zheltovodov et al., 1990a
ECC	2.9	8.0×10^4	Zheltovodov et al., 1990a
ECC	2.9	1.94×10^5	Zheltovodov et al., 1987; Zheltovodov et al., 1990b
ECC	2.88	2.0×10^4	Present computation
FPBL	2.88	1.33×10^5	Zheltovodov et al., 1990b

Results

The structure of the flowfield is shown in Figs. 4 and Fig. 5 which display the mean static pressure and streamlines at $z = \delta$. The flow expands around the first corner, and recompresses at the second corner through a shock which separates the boundary layer as evident in Fig. 5. The flowfield structure is in good agreement with the results of Zheltovodov et al., 1987; Zheltovodov and Schuelein, 1988; Zheltovodov et al., 1990a and Zheltovodov et al., 1990b which are shown qualitatively in Fig. 1.

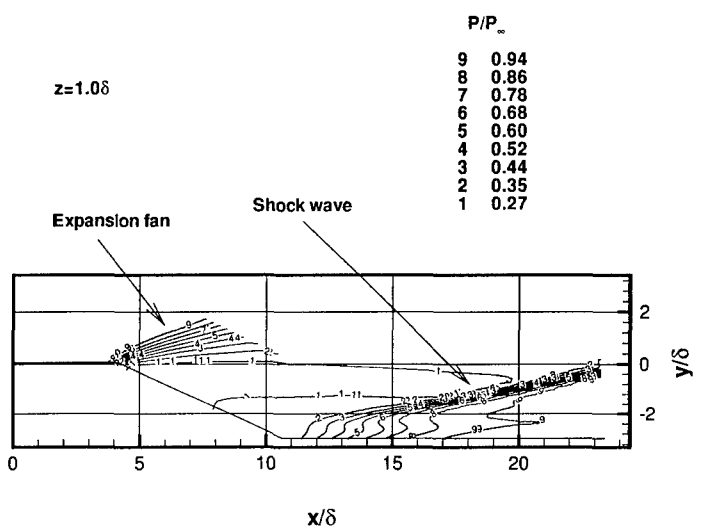

Figure 4. Mean static pressure (S is separation, A is attachment)

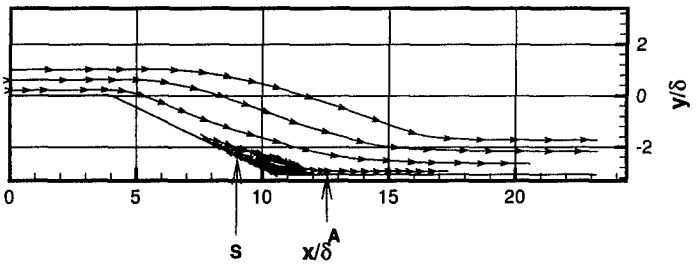

Figure 5. Mean streamlines (S is separation, A is attachment)

The mean velocity profiles in the x-direction are shown in Fig. 6 at $x = 2\delta$ and $x = 6\delta$, where x is measured from the inflow along the direction of the inflow freestream velocity (Fig. 4). The abscissa is the component of velocity locally parallel to the wall, and the ordinate is the distance measured normal to the wall. The first profile is upstream of the expansion corner which is located at $x = 4\delta$, and the second is downstream of the expansion fan and upstream of the separation point. The computed mean velocity profile at the first location is slightly fuller than the experiment. This is consistent with the experimentally observed dependence of the exponent n in the power-law $U/U_\infty = (y/\delta)^{1/n}$ on the Reynolds number. The second profile shows a significant acceleration of the flow in the outer portion of the boundary layer due to the expansion.

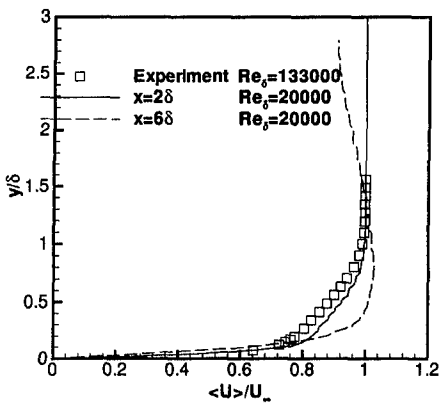

Figure 6. Mean velocity

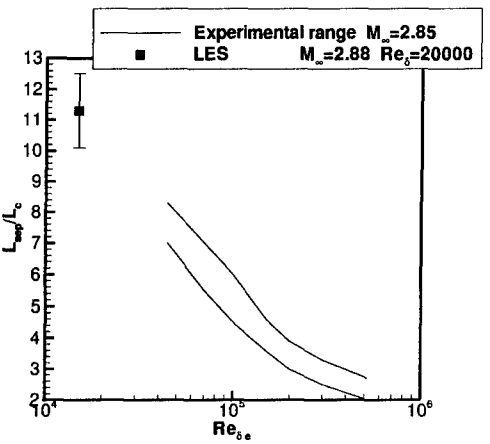

Figure 7. Separation length

Zheltovodov and Schuelein, 1988 and Zheltovodov et al., 1993 developed an empirical correlation for the separation length (defined as the minimum distance between the mean separation and attachment points on the wall) in the expansion-compression corner interaction. The scaled separation length L_{sep}/L_c is observed experimentally to be a function of Re_δ where the characteristic length (L_c) is defined by

$$L_c = \delta_e (p_2/p_{pl})^{3.1}/M_e^3 \tag{9}$$

where δ_e is the incoming boundary layer thickness (upstream of the expansion corner), p_2 is the pressure after the shock in inviscid flow, p_{pl} is the plateau pressure from the empirical formula $p_{pl} = p_e(\frac{1}{2}M_e + 1)$ where p_e and M_e are the static pressure and freestream Mach number upstream of the compression corner and downstream of the expansion fan. In the computation, the location is taken to be $x = 6\delta$. The values of M_e and p_2 have been computed using inviscid theory. Also, $Re_{\delta e} = 1.8 \times 10^4$ for LES ($Re_{\delta e} = \rho_e U_e \delta_e/\mu_e$, where ρ_e, U_e and μ_e are computed using inviscid theory). The experimental data correlation of Zheltovodov and Schuelein, 1988 and the computed result[1] for the scaled separation length is shown in Fig. 7. The computed value is consistent with a linear extrapolation of the expermental data.

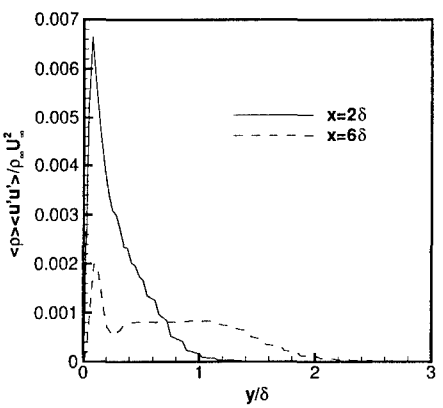

Figure 8. Reynolds streamwise stress

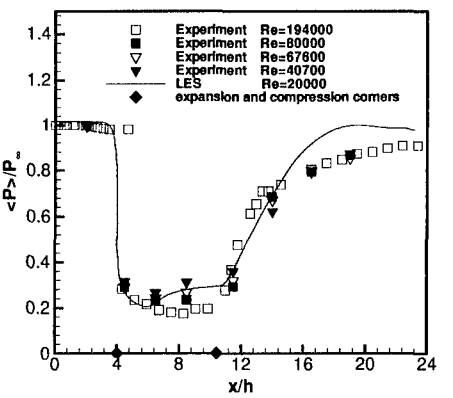

Figure 9. Surface pressure

The surface pressure profile in Fig. 9 displays a pressure plateau on the compression face generated by the separation bubble. The exper-

[1]The uncertainty in the computed value of L_{sep}/L_c is associated with the uncertainty in determining δ_e. We have used the streamwise Reynolds stress ($< \rho >< u'u' >$) to determine δ_e (Fig. 8), where u' is the fluctuating velocity parallel to the wall.

iments exhibit a trend of increase in the size of the pressure plateau region with decreasing Reynolds number. The experimental data at the lowest Reynolds number ($Re_\delta = 4.1 \times 10^4$) shows close agreement with the computed results for $Re_\delta = 2 \times 10^4$ for the location, extent and magnitude of the pressure plateau. Moreover, the shape of the experimental pressure plateau shows little variation for $Re_\delta \leq 6.8 \times 10^4$, thus suggesting that the computed pressure plateau region (for $Re_\delta = 2 \times 10^4$) is accurate. The computed recovery of the surface pressure is more rapid than in the experiment, however.

The computed and experimental mean skin friction coefficient $c_f = \tau_w / \frac{1}{2}\rho_\infty U_\infty^2$ are shown in Fig. 10. The computed separation and attachment points are evident. The skin friction rises rapidly downstream of attachment. The computed results at $Re_\delta = 2 \times 10^4$ are in close agreement with the experimental data at $Re_\delta = 8.0 \times 10^4$ and 1.94×10^5 in the region downstream of reattachment.

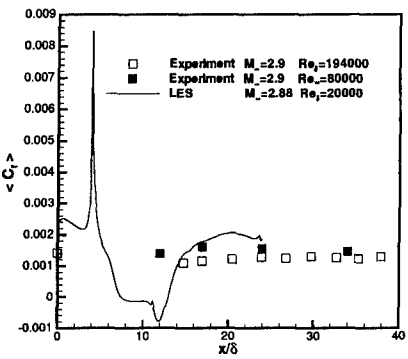

Figure 10. Skin friction coefficient

Summary

An unstructured grid Large Eddy Simulation methodology has been validated for complex compressible turbulent flows. The methodology is based on the MILES concept wherein the inherent dissipation of the monotone inviscid flux algorithm provides the energy transfer from the resolved to the subgrid scales. The methodology has been validated by comparison with experiment for a variety of supersonic turbulent flows including a turbulent boundary layer and an expansion-compression corner at Mach 3.

Acknowledgments

The research is supported by AFOSR Grant No. F49620-99-1-0008 monitored by R. Herklotz, L. Sakell, J. Schmisseur and S. Walker.

References

Adams, N. (1998). Direct Numerical Simulation of Turbulent Compression Ramp Flow. *Theoretical and Computational Fluid Dynamics*, 12:109–129.

Boris, J., Grinstein, F., Oran, E., and Kolbe, R. (1992). New Insights into Large Eddy Simulation. *Fluid Dynamics Research*, 10:199–228.

Chernyavsky, B., Yan, H., and Knight, D. (2001). Analyses of Some Numerical Issues in Compressible LES. AIAA Paper 2001-0436.

Dussauge, J. and Gaviglio, J. (1987). The Rapid Expansion of a Supersonic Turbulent Flow: Role of Bulk Dilatation. *Journal of Fluid Mechanics*, 174:81–112.

Fureby, C. and Grinstein, F. (1999). Monotonically Integrated Large Eddy Simulation of Free Shear Flows. *AIAA Journal*, 37:544–556.

Fureby, C. and Grinstein, F. (2000). Large Eddy Simulation of High Reynolds Number Free and Wall Bounded Flows. AIAA Paper No. 2000-2307.

Galperin, B. and Orszag, S., editors (1993). *Large Eddy Simulation of Complex Engineering and Geophysical Flows*. Cambridge University Press.

Ghosal, S. (1999). Mathematical and Physical Constraints on Large Eddy Simulation of Turbulence. *AIAA Journal*, 37(4):425–433.

Grinstein, F. and Fureby, C. (1998). Monotonically Integrated Large Eddy Simulation of Free Shear Flows. AIAA Paper No. 98-0537.

Grinstein, F. F. (1996). Dynamics of Coherent Structures and Transition to Turbulence in Free Square Jets. AIAA Paper No. 96-0781.

Knight, D. and Degrez, G. (1998). Shock Wave Boundary Layer Interactions in High Mach Number Flows – A Critical Survey of Current CFD Prediction Capabilities. AGARD AR-319, Volume 2.

Knight, D., Zhou, G., Okong'o, N., and Shukla, V. (1997). Large Eddy Simulation of Compressible Flows Using Unstructured Grids. In *First AFOSR Conference on DNS/LES*. Louisiana Tech University.

Knight, D., Zhou, G., Okong'o, N., and Shukla, V. (1998). Compressible Large Eddy Simulation Using Unstructured Grids. AIAA Paper 98-0535.

Lesieur, M. and Métais, O. (1996). New Trends in Large-Eddy Simulations of Turbulence. In *Annual Review of Fluid Mechanics*, volume 28, pages 45–82. Annual Reviews, Inc.

Lund, T., Wu, X., and Squires, K. (1998). Generation of Turbulent Inflow Data for Spatially- Developing Boundary Layer Simulations. *Journal of Computational Physics*, 140:233–258.

Martin, M., Piomelli, U., and Candler, G. (1999). A Priori Tests of SGS Models in Compressible Turbulence. 3rd ASME/JSME Joint Fluids Engineering Conference.

Okong'o, N. and Knight, D. (1998a). Accurate Three-Dimensional Unsteady Flow Simulation Using Unstructured Grids. AIAA Paper 98-0787.

Okong'o, N. and Knight, D. (1998b). Compressible Large Eddy Simulation Using Unstructured Grids: Channel and Boundary Layer Flows. AIAA Paper 98-3315.

Okong'o, N., Knight, D., and Zhou, G. (2000). Large Eddy Simulations Using an Unstructured Grid Compressible Navier-Stokes Algorithm. *International Journal of Computational Fluid Dynamics*, 13:303–326.

Oran, E. and Boris, J. (1993). Computing Turbulent Shear Flows - A Convenient Conspiracy. *Computers in Physics*, 7(5):523–533.

Rizzetta, D. and Visbal, M. (2001). Large Eddy Simulation of Supersonic Compression Ramp Flows. AIAA Paper 2001-2858.

Rizzetta, D., Visbal, M., and Gaitonde, D. (2000). Direct Numerical and Large-Eddy Simulation of Supersonic Flows by a High-Order Method. AIAA Paper 2000-2408.

Settles, G. and Dolling, D. (1990). Swept Shock / Boundary-Layer Interactions - Tutorial and Update. AIAA Paper 90-0375.

Smith, D. and Smits, A. (1997). The Effects of Successive Distortion on a Turbulent Boundary Layer in a Supersonic Flow. *Journal Fluid Mechanics*, 351:253–288.

Stephen, A., Mo, S., and Gregory, S. (1998). The Effects of Expansion on the Turbulence Structure of Compressible Boundary Layers. *J. Fluid Mechanics*, 367:67–105.

Urbin, G. and Knight, D. (1999). Compressible Large Eddy Simulation using Unstructured Grid: Supersonic Boundary Layer. In *Recent Advances in DNS and LES*, pages 443–458, Kluwer Academic Publishers.

Urbin, G. and Knight, D. (2001). Large Eddy Simulation of a Supersonic Boundary Layer Using an Unstructured Grid. *AIAA Journal*, 39(8):1288–1295.

Urbin, G., Knight, D., and Zheltovodov, A. (1999). Compressible Large Eddy Simulation Using Unstructured Grids: Supersonic Turbulent Boundary Layer and Compression Corner. AIAA Paper 99-0427.

Urbin, G., Knight, D., and Zheltovodov, A. (2000). Large Eddy Simulation of Supersonic Compression Corner Part I. AIAA Paper 2000-0398.

Yan, H., Urbin, G., Knight, D., and Zheltovodov, A. (2000). Compressible Large Eddy Simulation using Unstructured Grid: Supersonic Boundary Layer and Compression Ramps. In *10th International Conference on Methods of Aerophysical Research*, pages 215–224, Novosibirsk, Russia.

Zheltovodov, A. (1996). Shock Waves / Turbulent Boundary Layer Interactions - Fundamental Studies and Applications. AIAA Paper 96-1977.

Zheltovodov, A., Borisov, A., Knight, D., Horstman, C., and Settles, G. (1992). The Possibilities of Numerical Simulation of Shock Waves / Boundary Layer Interaction in Supersonic and Hypersonic Flows. In *Proceedings of the International Conference on Methods of Aerophysical Research. Part 1*, pages 164–170. Russian Academy of Sciences, Siberian Division, Novosibirsk.

Zheltovodov, A., Mecler, L., and Schuelein, E. (1987). Pecularities of Development of Separated Flows in Compression Corners After the Expansion Fans. ITAM Preprint 10-87. In Russian.

Zheltovodov, A. and Schuelein, E. (1988). Peculiarities of Turbulent Separation Development in Disturbed Boundary Layers. *Modelirovaniye v Mekchanike*, 2(1):53–58. Novosibirsk (in Russian).

Zheltovodov, A., Schuelein, E., and Horstman, C. (1993). Development of Separation in the Region of Interaction of Shock Wave with Turbulent Boundary Layer Disturbed by Expansion. *Journal of Applied Mechanics and Technical Physics*, 3:58–68. in Russian.

Zheltovodov, A., Trofimov, V., Filippova, E., and Takovlev, Y. (1990a). Influence of Turbulence Change on the Heat Exchange Under the Conditions of Supersonic Separated Flows. In *Abstracts: IUTAM Symposium on Separated Flows and Jets*, pages 273–274. USSR Academy of Sciences, Siberian Division, Novosibirsk.

Zheltovodov, A., Trofimov, V., Schuelein, E., and Yakovlev, V. (1990b). An Experimental Documentation of Supersonic Turbulent Flows in the Vicinity of Forward- and Backward-Facing Ramps. ITAM Report 2030.